Applied Catalysis B: Environmental 163 (2015) 40–49

Contents lists available at ScienceDirect

Applied Catalysis B: Environmental

journal homepage: www.elsevier.com/locate/apcatb

Visible light activity of rare earth metal doped (Er^{3+}, Yb^{3+} or Er^{3+}/Yb^{3+}) titania photocatalysts

Joanna Reszczyńska[a,e], Tomasz Grzyb[b], Janusz W. Sobczak[c], Wojciech Lisowski[c], Maria Gazda[d], Bunsho Ohtani[e], Adriana Zaleska[a,*]

[a] Department of Chemical Technology, Faculty of Chemistry, Gdansk University of Technology, 80-233 Gdansk, Poland
[b] Department of Rare Earths, Faculty of Chemistry, Adam Mickiewicz University, 60-780 Poznan, Poland
[c] Mazovia Center for Surface Analysis, Institute of Physical Chemistry, Polish Academy of Sciences, 01-224 Warsaw, Poland
[d] Department of Solid State Physics, Faculty of Applied Physics and Mathematics, Gdansk University of Technology, 80-952 Gdansk, Poland
[e] Catalysis Research Center, Hokkaido University, Sapporo 001-0021, Japan

ARTICLE INFO

Article history:
Received 10 April 2014
Received in revised form 11 June 2014
Accepted 3 July 2014
Available online 15 July 2014

Keywords:
Heterogeneous photocatalysis
Doped-TiO_2
Erbium
Ytterbium
Action spectra analysis

ABSTRACT

A series of Er^{3+}-TiO_2, Yb^{3+}-TiO_2 and Er^{3+}/Yb^{3+}-TiO_2 photocatalysts were obtained via sol–gel method, using lanthanides precursor ranging from 0.25 to 10 mol%. The experiments demonstrated that phenol in aqueous solutions was successfully degraded under visible light ($\lambda > 450$ nm) using Er/Yb-TiO_2. The as-prepared samples were characterized by X-ray diffraction (XRD), X-ray photoelectron emission spectroscopy (XPS), UV–vis absorption measurement, BET surface area analysis and luminescent spectroscopy. XPS analysis revealed that erbium and ytterbium were present in the form of oxides. The sample showing the highest photoactivity was in the form of anatase, its surface area equalled to 125 m^2/g, average crystals size was 13 nm, and it was prepared introducing 1 mol% of Yb^{3+} into reaction medium. 3 h of irradiation resulted in 89% of phenol degradation under visible light. Action spectra analysis performed for the selected Er/Yb-TiO_2 samples, revealed that irradiation from 420 to 475 nm is responsible for visible light photoactivity.

1. Introduction

In recent years, environment contamination, such as water and air pollution, has become a very serious problem all over the world. Photocatalysis is known as a very promising method in solving the problems for it is an environmentally friendly technique [1,2]. Titanium dioxide is one special oxide semiconductor that has been vastly studied, owing to its multifunctionality [3]. Even though TiO_2 is sensitive only to UV light due to its large band gap and has low quantum efficiency, which is due to the fast recombination rate of photogenerated electron–hole pairs, TiO_2 is still preferred as an ideal candidate to be developed as a visible light active photocatalyst because of its strong oxidation capacity, physical and chemical stability and low cost of production [4–7]. For a long time, much attention has been drawn to the preparation of TiO_2 modified with metal nanoparticles exhibiting reactivity under visible light ($\lambda > 400$ nm), which should allow the use of a larger part of the solar spectrum or even of poor interior light illumination [8]. In recent years TiO_2 doped with rare earth (RE) metals has proved to be an efficient method to improve the photocatalytic properties of TiO_2 because the f-orbitals of the lanthanide ions can form complexes with various Lewis bases and thus, concentrate the substrates onto the TiO_2 surface [9–11]. Recently, most of the interest in luminescent rare earth ions has focused on Er^{3+} due to its unique electronic and optical properties [12]. Another lanthanide ion: Yb^{3+} is one of the best known suitable sensitizer of Er^{3+} luminescence under NIR (near infrared) radiation, due to its particular electronic configuration, a unique long lifetime of excited state and a large absorption cross section for the $^2F_{7/2} \rightarrow {}^2F_{5/2}$ transitions at around 1 μm. This makes the Yb^{3+}–Er^{3+} couple a very efficient upconversion (UC) system [13].

There are lot of reports on Er^{3+} or Er^{3+}/Yb^{3+}-doped TiO_2 [14–40], but mainly described only luminescent properties [14–30] or focused on photocatalytic activity without discussing luminescence properties [33–37]. In most reports, photocatalytic properties of such samples were measured using dyes as model substances in photodegradation tests [31–35]. Dyes are not recommended to use as model compounds, due to their absorption, especially in the visible light range, large

* Corresponding author. Tel.: +48 58 347 24 37; fax: +48 58 347 20 65.
E-mail addresses: adriana.zaleska@pg.gda.pl, azaleska@chem.univ.gda.pl (A. Zaleska).

http://dx.doi.org/10.1016/j.apcatb.2014.07.010
0926-3373/

photoabsorption coefficient and complicated mechanism of degradation [41].

According to our best knowledge, only a few papers dealing with photocatalytic activity for Er^{3+} or Yb^{3+}-doped TiO_2, estimated using other organic compounds than dyes. Hou et al. [38] prepared Fe/Er-TiO_2 photocatalysts by a facile solvothermal method. The experimental results indicated an improved photocatalytic activity of Fe/Er-TiO_2 for bisphenol A degradation compared to pure TiO_2, Er-TiO_2, Fe-TiO_2 and Degussa P25 (P25) under visible light irradiation. Reszczynska et al. [39] used the sol–gel method to synthesize Er^{3+} and Yb^{3+} modified TiO_2 nanoparticles. Photocatalytic activity was estimated by measuring the rate of phenol decomposition in an aqueous solution. It was observed that the dopant amount affected photocatalytic activity of a semiconductor. Obregon et al. [40] synthesized erbium-doped TiO_2 materials by hydrothermal method having good photoactivities for the liquid-phase degradation of phenol and methylene blue dye and the gas phase of toluene. They observed ultraviolet upconversion fluorescence under 980 nm excitation. In the first two reports upconversion effect of the samples was not measured. In the last one the authors did not investigate the influence of Yb^{3+} on Er^{3+}-TiO_2 photocatalysts.

The aim of this work was to understand the effect of the dopant type and the amount of Er^{3+}, Yb^{3+} or Er^{3+}/Yb^{3+} ions doped TiO_2, on the structure, optical and luminescence properties, and their relation with the photocatalytic properties under visible light. RE^{3+}-TiO_2 were prepared by the sol–gel method, which is a cheap, simple and reproducible way of synthesis. Surface properties of Yb^{3+}, Er^{3+} or Yb^{3+}/Er^{3+} TiO_2 were characterized using BET method, XRD, XPS, UV–vis and luminescence spectroscopy. The photocatalytic properties were investigated by employing the photodegradation of phenol and acetic acid in aqueous phase as a model pollutant. To understand the excitation mechanism of as-prepared samples, the effect of irradiation wavelength on apparent quantum efficiency (action spectra analysis) was investigated for the selected sample. To our best knowledge, complementary characteristics of such composites, including photoactivity and mechanism discussion, was done for the first time.

2. Experimental

2.1. Materials and apparatus

Titanium(IV) isopropoxide (97%, TIP) was purchased from Sigma–Aldrich and used as titanium source for the preparation of TiO_2 nanoparticles. $Er(NO_3)_3{\cdot}6H_2O$ and $Yb(NO_3)_3{\cdot}6H_2O$ salts were freshly prepared by the reaction of Er_2O_3 and Yb_2O_3 with nitric acid. Er_2O_3 (99.9%) and Yb_2O_3 (99.9%) were obtained from Sigma–Aldrich, acetic acid and ethanol (Poch S.A., Poland) while TiO_2 P25 from Evonik, Germany (surface area 50 m^2/g, crystalline composition: 80% anatase, 20% rutile). All the chemicals were used as received without further purification. Deionized water was used for all the reactions and treatment processes.

X-ray diffraction patterns (XRD) were recorded on an X-ray diffractometer (Xpert PRO-MPD, Philips) with Cu target Kα-ray ($\lambda = 1.5404$ Å) in the range $2\theta = 20$–68° and 20–105° for phase analysis and unit cell parameters determination, respectively. The patterns were analyzed by Rietveld refinement method using the version of the program LHPM [42]. The pseudo-Voigt profile function was applied. As the initial data for the analysis, unit cell parameters of the anatase (space group no. 141, I41/amd) [43] were used. The crystallite size was estimated by Scherrer equation. The accuracy of the grain size analysis was estimated to be about 20%. Nitrogen adsorption–desorption isotherms were recorded at liquid nitrogen temperature (−197 °C) on a Micromeritics Gemini V (model 2365) and the specific surface areas were determined by the Brunauer–Emmett–Teller (BET) method in the relative pressure (p/p_0) range of 0.05–0.3. All the samples were degassed at 200 °C prior to nitrogen adsorption measurements. To characterize the light-absorption properties of modified photocatalysts, diffuse reflectance (DRS) spectra were recorded. The measurements were carried out on UV-Vis Thermo model: Nicolet Evolution 220 with ISA-220 integrating sphere equipped with an integrating sphere and $BaSO_4$ was used as the reference. All XPS spectra were recorded on a Physical Electronics PHI 5000 Versa Probe scanning spectrometer using monochromatic Al K_α X-rays working with power 25 W. X-ray beam was focused to diameter 100 μm, the measured area was defined as a 250 μm square. Binding energies (BE) of all the detected XPS peaks were referenced to the Ti $2p_{3/2}$ core level (BE = 458.6 eV). The hemispherical electron energy analyzer was operated at a pass energy 23.50 eV for all high-resolution measurements. Spectroscopic properties (emission and luminescence lifetimes) were measured on Quanta Master™ 40 spectrophotometer equipped with Opolette 355LD UVDM tunable laser as an excitation source with the repetition rate 20 Hz and a Hamamatsu R928 photomultiplier as a detector.

2.2. Preparation of RE^{3+}-TiO_2 photocatalysts

The sol–gel method was used for the preparation of RE^{3+}-TiO_2 nanocrystals. In a typical procedure 10.2 mL TIP was first dissolved in 48 mL ethanol and 6 mL acetic acid. After 10 min of stirring 3 mL of deionized water was dropped into the solution under vigorous agitation. Then, a certain amount of freshly prepared $Er(NO_3)_3$ and $Yb(NO_3)_3$ was added and the sol was stirred for one more hour. The obtained gel was dried at 60 °C for 20 h in a vacuum oven and ground to obtain powder. The heat treatment of 400 °C for 2.5 h in the air was applied to the sample. The concentration of metal precursors, which varied from 0.25 to 10 mol% was related to the concentration of TIP in the sol–gel system. For comparison the TiO_2 nanocrystals without any RE ions were also synthesized under the same preparation process. The description of the prepared photocatalysts is shown in Table 1.

2.3. Adsorption capacity

Adsorption is an indispensable step in any heterogeneous photocatalytic reaction. To investigate the adsorption behavior of pure TiO_2 and RE^{3+}-TiO_2 photocatalysts, adsorption tests were performed in the dark conditions. A fixed amount of the photocatalyst (50 mg) was added to phenol solution (0.21 mM, 5.0 mL) and mixed (500 rpm) without any illumination. The temperature of the suspension was maintained at 15 ± 5 °C until equilibrium was reached (30 min). Initial and equilibrium phenol concentration was determined using a reverse phase HPLC system. The HPLC system included a Shodex ODP2 HP-4E reversed-phase column (4.6 mm in inner diameter; 250 mm in length, Showa Denko) with a mobile phase of acetonitrile (70%)–water (29.5%)–phosphoric acid (0.5%); a flow rate of 0.5 mL/min and a UV detector at 254 nm.

2.4. Phenol decomposition under polychromatic irradiation

The visible light-driven activity of the obtained samples was estimated by measuring the rate of phenol decomposition in an aqueous solution. Phenol was selected as a model pollutant because it is a non-volatile and common contaminant present in industrial wastewaters [44]. The mechanism of phenol decomposition is also well established both under UV and visible-light irradiation [45]. For photocatalytic reaction in an aqueous phase, RE^{3+}-TiO_2 powder (50 mg) was suspended in phenol solution (0.21 mM, 5.0 mL). The experiment was placed in pyrex tubes. After 30 min in the dark, the suspension was photoirradiated with a 400 W Xenon

Table 1
Labeling, dopant type and amount and selected physicochemical properties of RE^{3+}-TiO_2 photocatalysts prepared by sol–gel method.

Sample label	Metal precursor used during preparation		Assumed content of dopant (mol%)		Color of the photocatalyst	S_{BET} (m^2/g)	Crystals size (nm)
TiO_2_Pure	None		None		White	118	15.0
TiO_2_Er(0.25)	Er_2O_3		0.25 Er		White	126	13.0
TiO_2_Er(0.5)	Er_2O_3		0.5 Er		White	113	14.6
TiO_2_Er(1.0)	Er_2O_3		1.0 Er		Light pink	123	15.5
TiO_2_Yb(0.25)	Yb_2O_3		0.25 Yb		White	119	14.0
TiO_2_Yb(0.5)	Yb_2O_3		0.5 Yb		White	132	15.5
TiO_2_Yb(1.0)	Yb_2O_3		1.0 Yb		White	125	13.2
TiO_2_Er(0.25)_Yb(0.5)	Er_2O_3	Yb_2O_3	0.25 Er	0.5 Yb	White	131	8.9
TiO_2_Er(0.5)_Yb(0.5)	Er_2O_3	Yb_2O_3	0.5 Er	0.5 Yb	White	140	10.2
TiO_2_Er(2)_Yb(10)	Er_2O_3	Yb_2O_3	2.0 Er	10 Yb	Light pink	132	13.4

lamp under magnetic stirring (500 rpm). The temperature of the suspension during photoirradiation was maintained at 15 ± 5 °C using a thermostatically controlled water bath. The optical path included a water filter and a glass filter (Y48, Asahi Techno Glass, 450 nm), which transmitted light of the wavelength longer than 450 nm. Aqueous suspension (0.2 mL) was collected at regular time periods during irradiation and filtered through syringe filters (Ø = 0.1 μm) to remove photocatalyst particles and analyzed using a reverse phase HPLC system. The HPLC system included a Shodex ODP2 HP-4E reversed-phase column (4.6 mm in inner diameter; 250 mm in length, Showa Denko) with a mobile phase of acetonitrile (70%)–water (29.5%)–phosphoric acid (0.5%); a flow rate of 0.5 mL/min and a UV detector at 254 nm.

2.5. Acetic acid decomposition – action spectra measurements

For the selected photocatalyst the action spectra measurements were investigated. Each photocatalyst powder (30 mg) was suspended in aqueous solution (3.0 mL) containing 5.0 vol% of acetic acid and placed in a rectangular quartz cell (10 mm square and 50 mm in height), then irradiated at monochromatic wavelengths for 150 min using a diffraction grating-type illuminator (Jasco, CRM-FD), equipped with a 300 W Xenon lamp (Hamamatsu, C2578-02). The light intensity was measured by an optical power meter (HIOKI 3664). During the experiments, the reaction mixtures were continuously stirred. During the irradiation, every 20 min a portion (0.2 mL) of the gas phase of the reaction mixture was withdrawn with a syringe and subjected to gas chromatographic analysis of carbon dioxide chromatography (Shimadzu GC-8A). The wavelength-dependent apparent quantum efficiency was calculated as the ratio of the rate of electron consumption from the rate of CO_2 generation to the flux of incident photons, assuming that four photons are required, according to the stoichiometry of the reaction:

$$CH_3COOH + 2O_2 = 2CO_2 + 2H_2O$$

3. Results and discussion

3.1.1. UV–vis diffuse reflectance spectra

To study the optical absorption properties of TiO_2 doped with Er^{3+}, Yb^{3+} and Er^{3+}/Yb^{3+} and the undoped one, the diffusive reflectance spectra (DRS) in the range of 350–700 nm were investigated as shown in Fig. 1. P25 was chosen as a reference sample and it is clearly seen that it shows absorption only in the UV region. Each sample has a broad intense absorption below 390 nm, which is the characteristic absorption corresponding to the excitation of electrons from the valence band to the conduction band in anatase TiO_2 [46]. All doped powders showed a slight shift of their absorption edge into the visible light compared to P25. The DRS results showed that when the smallest amount of the dopant was chosen then the optical absorption edge was shifted more to the red direction. The red shift in the band gap transition, existed due to the charge transfer transition between TiO_2 and RE^{3+} intra-4f electrons [31]. Furthermore, it can be seen that there are absorption peaks located at 451, 475, 524 and 655 nm, which can be attributed to the transition from the $^4I_{15/2}$ ground state to the excited states of the erbium ions $^4F_{3/2,5/2}$, $^4F_{7/2}$, $^2H_{11/2}$ and $^4F_{9/2}$ [30,35]. The intensity of erbium ions absorption bands was found to increase with increasing the rare earth content. According to Judd–Ofelt theory of parity-forbidden electric-dipole transitions of rare earth ions, the energy states of the Er^{3+} should be effectively perturbed by the odd terms of the Hamiltonian of the weak crystal field. Although 4f energy electrons have been partially screened by $5s^2$ and $5p^6$ electron shells, the perturbations can still cause permitted transitions of 4f elections between 4f energy levels [47]. The transitions of 4f electrons of Er^{3+} favor the separation of photogenerated electron–hole pairs. That is helpful for the improvement of photocatalytic activity under visible light [33].

3.2. X-ray diffraction and BET surface area

Powder X-ray diffraction (XRD) was used to verify the crystalline phase of synthesized doped TiO_2 and to estimate the crystallite size. The XRD patterns of the examined samples are shown in Fig. 2. All the patterns indicate the formation of the single anatase phase. Only in the case of the sample doped with 10% of Yb^{3+} and 2% of Er^{3+} a very small diffraction peak indicating the presence of unreacted ytterbium oxide was detected, however, the scale of Fig. 2 does not allow to see it. The average particle size, determined on the base of Scherrer equations, ranged from 8.9 to 15.5 for TiO_2_Er(0.25)_Yb(0.5) and TiO_2_Yb(0.5), respectively. For undoped TiO_2 the particle size was 15.0 nm (Table 1). The increase in the concentration of doped lanthanide ions could increase the size of TiO_2 nanocrystals. Similar average particle size of Er^{3+}-TiO_2 was observed by Castañeda-Contreras et al. [31]. Unit cell parameters of doped anatase depend on the ionic radius of a dopant, its valence state, concentration of cation and anion vacancies and on the anatase particle size. Nonlinear size dependence of unit cell parameters of anatase particles of the diameter below approximately 10 nm was reported [48,49]. Both contraction and expansion of unit cell was observed. For example, in the case of anatase prepared via sol–gel or hydrolysis method, which lead to forming Ti vacancies, the unit cell expansion was observed [48]. Crystallite sizes of doped titanium oxide studied in this work are in the range between 8.9 and 15.5 nm. Therefore, it could be assumed that for relatively big crystallite size, such as 14–15 nm, unit cell parameters of the samples are not influenced by the grain size. In these cases a possible influence of ionic radius of the dopants on the unit cell volume should be considered. Ionic radii of Yb^{3+} (99 pm) and Er^{3+} (88 pm) are bigger than these of Ti^{4+} (61 pm) which means that these ions

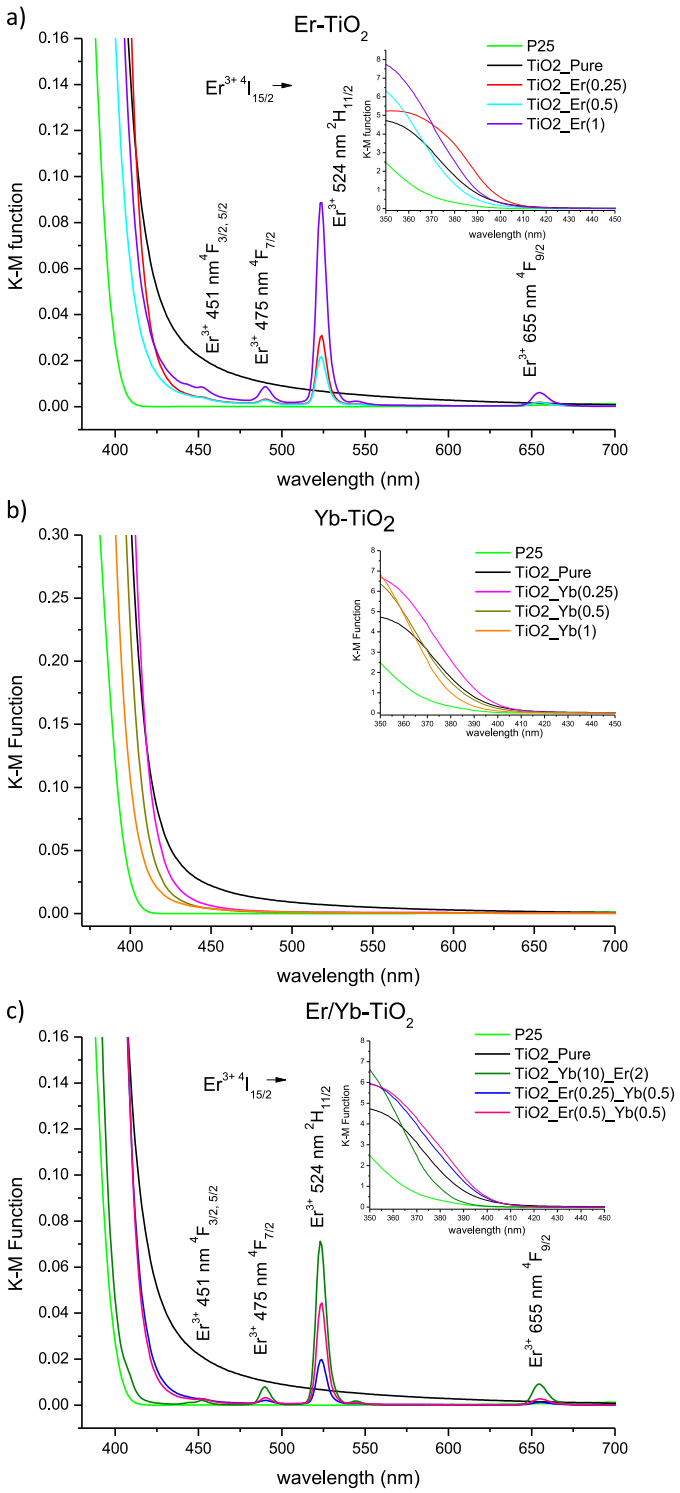

Fig. 1. UV–vis Kubelka–Munk absorption of RE^{3+}-TiO_2 photocatalysts compared to P25 and pure TiO_2 (a) Er-TiO_2; (b) Yb-TiO_2; (c) Er/Yb-TiO_2.

either do not enter the crystal lattice of anatase or introduce a considerably high disorder into the lattice. It should be stressed that there is no agreement in literature whether rare earth ions substitute titanium in the lattice. For example, Yan et al. [46] suggested that the doped Yb^{3+} exist at the crystal boundary rather than in the inner structure of the TiO_2 crystal lattice. On the other hand, other authors, e.g. Antic et al. [51] and Luo et al. [50] reported the evidence of the incorporation of Eu^{3+} and Sm^{3+} ions into anatase matrix [51]. In order to determine possible influence of doping on

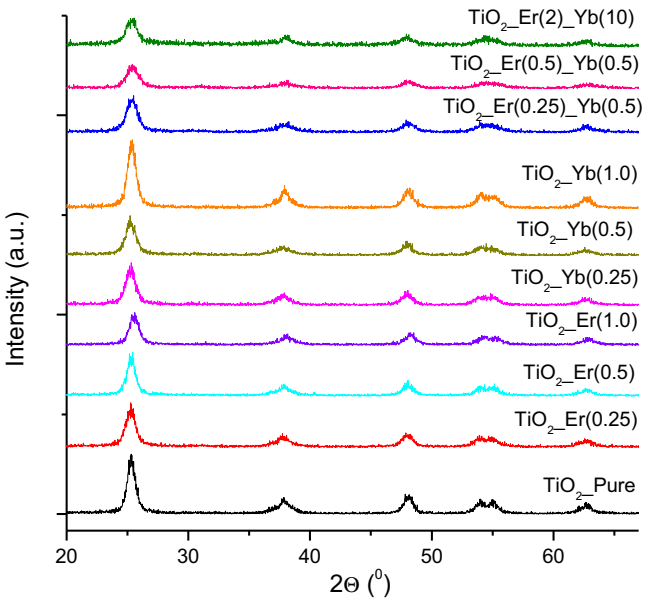

Fig. 2. XRD pattern of RE-TiO_2 photocatalysts prepared by sol–gel method.

Table 2
Unit cell parameters for selected TiO_2 samples. The value of *R* profile in all refinements was below 15%.

Sample	*a* (Å)	*c* (Å)	*V* (Å^3)
TiO_2_Pure	3.7846(4)	9.504(1)	136.12 ± 0.05
TiO_2_Er(0.5)	3.7852(7)	9.504(2)	136.16 ± 0.08
TiO_2_Er(1.0)	3.7863(3)	9.506(1)	136.27 ± 0.05
TiO_2_Yb(0.5)	3.7858(3)	9.506(1)	136.24 ± 0.05
TiO_2_Yb(1.0)	3.7871(8)	9.502(2)	136.28 ± 0.09
TiO_2_Er(0.5)_Yb(0.5)	3.7854(6)	9.501(2)	136.20 ± 0.07
TiO_2_Er(2)_Yb(10)	3.7960(5)	9.499(2)	136.88 ± 0.06

the unit cell parameters Rietveld analysis of the XRD patterns of selected TiO_2 samples were performed. The results are collected in Table 2. The observed titanium site occupancy was between 0.93 and 0.96. In this range of titanium deficiency no significant lattice strain has been observed [48]. The results indicate that there is a very small lattice expansion as a result of doping with either Er or Yb. Also in the case of co-doped samples the unit cell volume is larger than this of the undoped TiO_2. Moreover, the unit cell of titanium oxide doped with 10% of ytterbium and 2% of erbium has larger volume than these of TiO_2 doped with 1% of a rare earth element. However, the co-doped samples show lower crystallite sizes (between 8.9 and 13.4 nm), so that the reason for a unit cell volume increase cannot be unambiguously determined. What is more, the presence of Yb_2O_3 was detected in the XRD pattern. It indicates that the solubility limit of these elements in anatase is higher than 1% but lower than 10%. No systematic research on the solubility of rare earth elements in anatase has been published so far.

3.3. BET surface area and adsorption capacity

The BET surface areas for rare earth metal ions doped TiO_2 photocatalysts are listed in Table 1. The surface area was similar for all samples and ranged from 113 to 140 m^2/g. The highest BET surface area was observed for TiO_2_Er(0.5)_Yb(0.5) sample. The increase in the concentration of doped lanthanides could increase the TiO_2 BET surface area compared to pure TiO_2 nanoparticles. Er^{3+}/Yb^{3+} co-doped TiO_2 has higher BET surface area than Er^{3+} and Yb^{3+} mono-doped TiO_2. These results are in agreement with the literature reported previously. The surface area of Yb/TiO_2 was changed from 223 to 331 m^2/g after introducing Yb ions [52]. Higher

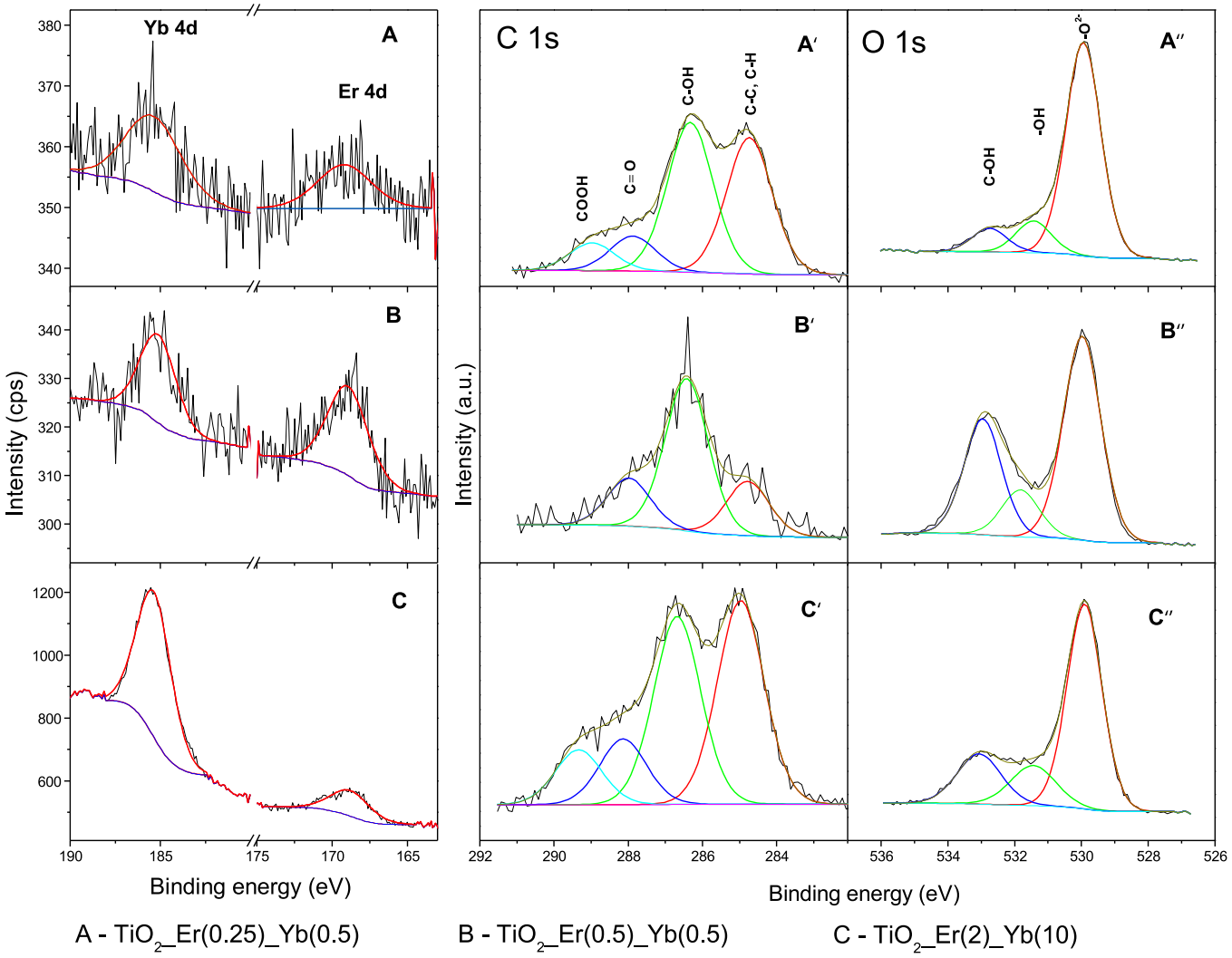

Fig. 3. XPS spectra of prepared photocatalysts modified by rare earth metals (Er/Yb-TiO_2).

specific surface areas can improve the adsorption ability of photocatalysts, because the photocatalytic activity strongly depends on the better adsorption of organic substrate and the interfacial charge transfer can also be improved [11]. To investigate the adsorption behavior of pure TiO_2 and RE^{3+}-TiO_2 photocatalysts, adsorption tests were performed in the dark. Adsorption of phenol after 30 min in the dark in the presence of pure and RE-doped TiO_2 nanoparticles are listed in Table 4. The results showed that RE^{3+}-TiO_2 photocatalysts had better adsorption capacity than pure TiO_2. The highest degree of adsorption (above 8%) were observed for samples TiO_2_Er(0.25), TiO_2_Er(0.5)_Yb(0.5) and TiO_2_Yb(1). Increase in the adsorption capacity was observed previously for TiO_2 modified with erbium in comparison to pure TiO_2 [33].

3.4. X-ray photoelectron spectroscopy analysis

Table 3 shows composition and chemical characters of elements incorporated into the surface layer of pure and RE-doped TiO_2 samples. The surface composition of Ti, O, C, Yb and Er was evaluated using the high-resolution (HR) Ti 2p, O 1s, C 1s, Yb 4d and Er 4d XPS spectra, respectively. The Ti 2p XPS spectrum can be resolved into two components at binding energies (BE) of 458.6 eV and 457.2 eV, which can be assigned to Ti^{4+} and Ti^{3+}, respectively [53,54]. Relative contribution of both components is presented in Table 3. Examination of the data clearly shows that Ti^{4+} is the dominant surface state. The largest contribution of Ti^{3+} species was found in TiO_2_Er(0.25) and TiO_2_Er(0.25)_Yb(0.5) samples.

It should be emphasized that XPS quantitative characterization of RE-doped Ti oxide samples is limited by the elemental detection range of XPS analysis. The escape depth of photoelectrons emitted from Ti $2p_{3/2}$, Yb 4d and Er 4d XPS states can be roughly estimated to be about 3.0, 1.5 and 1.45 nm, respectively [55]. Thus, the elemental composition, determined by XPS analysis, can be evaluated within the depth of TiO_2 samples. XPS analysis reveals relatively large carbon content in the surface layer of all analyzed samples. It is highly probable that carbon-like species in TiO_2 surface layers are formed as a result of the preparation procedure.

The chemical character of carbon and other elements detected within the surface layer of all RE-doped TiO_2 samples were identified from high-resolution XPS spectra. The analysis of HR spectra for the selected TiO_2 samples doped with various concentrations of Er and Yb is shown in Fig. 3. The deconvoluted XPS spectra of Yb 4d, Er 4d, C 1s and O 1s reveal the chemical character of Yb, Er, C and O, respectively for the samples: A-TiO_2_Er(0.25)_Yb(0.5), B–TiO_2_Er(0.5)_Yb(0.5) and C–TiO_2_Er(2)_Yb(10). Yb 4d and Er 4d XPS peak positions, located at BE of 1851–185.3 eV and 168.7–169.2 eV, respectively, indicate that Yb and Er states are to be attributed to Yb_2O_3 [56,57] and Er_2O_3 [57] oxides.

C 1s region can be deconvoluted for three to four peaks, at BE of 289.1–289.3 eV, 287.9–288.1 eV, 286.3–286.5 eV and

Table 3
Chemical composition of RE^{3+}-TiO_2 photocatalysts based on XPS analysis.

Sample label	Ti	Ti^{4+}		Ti^{3+}		O	C	RE	
		458.60 eV		457.00 eV				wt.%	
	wt.%	wt.%	% Ti	wt.%	% Ti	wt.%	wt.%	Er^{3+}	Yb^{3+}
TiO_2_Pure	23.7	23.3	98.2	0.4	1.8	49.2	27.1	0.0	0.0
TiO_2_Er(0.25)	21.7	21.0	97.7	0.7	2.3	46.8	31.3	0.30	0.0
TiO_2_Er(0.5)	29.6	29.2	98.8	0.3	1.2	46.0	24.1	0.29	0.0
TiO_2_Er(1)	18.2	18.0	98.5	0.3	1.5	48.0	33.3	0.44	0.0
TiO_2_Yb(0.25)	32.1	31.8	99.0	0.2	1.0	45.7	22.0	0.0	0.23
TiO_2_Yb(0.5)	32.1	31.8	98.0	0.3	2.0	44.7	22.8	0.0	0.40
TiO_2_Yb(1)	44.1	43.6	98.9	0.5	1.1	44.0	11.4	0.0	0.57
TiO_2_Er(0.25) Yb(0.5)	47.6	45.7	96.0	0.9	4.0	42.4	9.3	0.30	0.38
TiO_2_Er(0.5)_Yb(0.5)	34.2	33.4	97.4	0.9	2.6	45.7	19.3	0.46	0.36
TiO_2_Er(2) Yb(10)	36.4	36.3	99.6	0.1	0.4	42.1	11.6	1.85	7.78

Table 4
Photocatalytic activity of RE^{3+}-TiO_2 photocatalysts prepared by sol–gel method under visible irradiation.

Sample label	Efficiency of phenol adsorption of after 30 min in the dark condition (%)	Visible irradiation (λ > 450 nm)		
		Phenol degradation rate (μmol dm^{-3} h^{-1})	BQ formation rate (μmol dm^{-3} h^{-1})	Intermediate products
TiO_2_Pure	2.5	31.89	2.57	
TiO_2_Er(0.25)	13.9	39.77	1.40	
TiO_2_Er(0.5)	4.6	53.06	2.36	
TiO_2_Er(1)	7.6	50.77	3.03	General intermediate products: benzoquinone, short-chain compounds
TiO_2_Yb(0.25)	5.1	36.10	2.62	
TiO_2_Yb(0.5)	2.4	41.45	2.42	
TiO_2_Yb(1)	8.1	58.35	1.46	
TiO_2_Er(0.25)_Yb(0.5)	7.3	46.06	1.62	
TiO_2_Er(0.5)_Yb(0.5)	8.4	43.72	1.92	
TiO_2_Er(2)_Yb(10)	5.8	<detection limit	<detection limit	
P25	6.8	12.85	0.62	

284.7–284.9 eV, which can be assigned to COOH, C=O, C—OH, and C—C (aromatic and aliphatic) states, respectively [58]. O 1s peak can be composed of three different species, at BE of 529.9–530 eV, 531.5–531.8 eV and 532.8–533.0 eV, which can be described as TiO_x, Ti—OH and C—OH, respectively [59]. The presented results evidenced a large content of carbon–oxygen species coexisting with Ti- and RE-oxides on the surface of RE-doped Ti oxide samples.

3.5. Luminescence properties

Luminescence of doped-TiO_2 powders was measured under excitation wavelengths form UV, vis and NIR: 250, 451, 475, 524, 545, 655, 660, 978 and 1490 nm respectively, however, only 250 and 978 excitations were effective. Emission spectra are presented in Figs. 4 and 5. After excitation by 250 nm laser wavelength a broad emission band was measured for each sample. According to literature assignment, peak at 500 nm could be associated to oxygen vacancies with one trapped electron [40]. From this plot, it can be noticed that RE-TiO_2 exhibits general decrease in the emission intensity, which clearly indicates that the presence of lanthanides species induces hard suppression of the recombination process of photogenerated electrons and holes.

Besides UV-excited emission, synthesized materials were also analyzed in terms of upconversion luminescence. Upconversion is a non-linear optical process which can be obtained through the absorption of at least two photons, usually from the NIR spectral range and emission of light at a wavelength shorter than that of the excitation (anti-Stokes emission) [60]. This process is effective in lanthanides doped inorganic materials. The most studied and efficient are Er^{3+}, Ho^{3+} and Tm^{3+} ions as well as Yb^{3+}/Er^{3+}, Yb^{3+}/Tm^{3+} and Yb^{3+}/Ho^{3+}pairs of ions [61,62]. Therefore, also in TiO_2 materials doped with Er^{3+} or Yb^{3+}/Er^{3+} ions upconversion should be visible. Indeed, after excitation by 978 nm laser beam, low intensive upconversion emission was observed, which is presented in Fig. 5.

Upconversion is possible in the case of Er^{3+} ion by the ground and excited state absorption mechanisms (GSA and ESA) [60]. This ion has a low intensive absorption band around 980 nm, connected with excitation from the ground $^4I_{15/2}$ state to $^4I_{11/2}$ excited state. Ions in their excited state can absorb another portion of energy approaching higher energetic levels which finally results in radiative relaxation with the emission of light.

Upconversion of Er^{3+} ions can be obtained by excitation wavelengths from visible to the IR range. Besides the most effective and

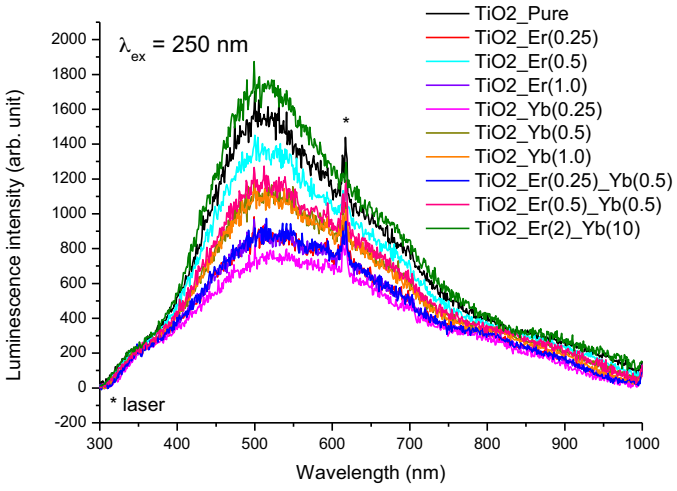

Fig. 4. Emission spectra of the TiO_2 samples doped with lanthanide ions under excitation of laser wavelength λ_{ex} = 250 nm.

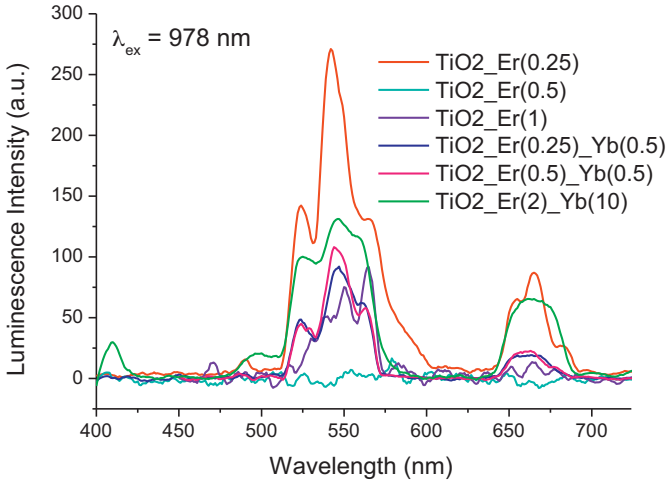

Fig. 5. Upconversion spectra of the TiO_2 samples doped with Er^{3+}or Er^{3+} and Yb^{3+} ions under excitation of laser wavelength λ_{ex} = 978 nm.

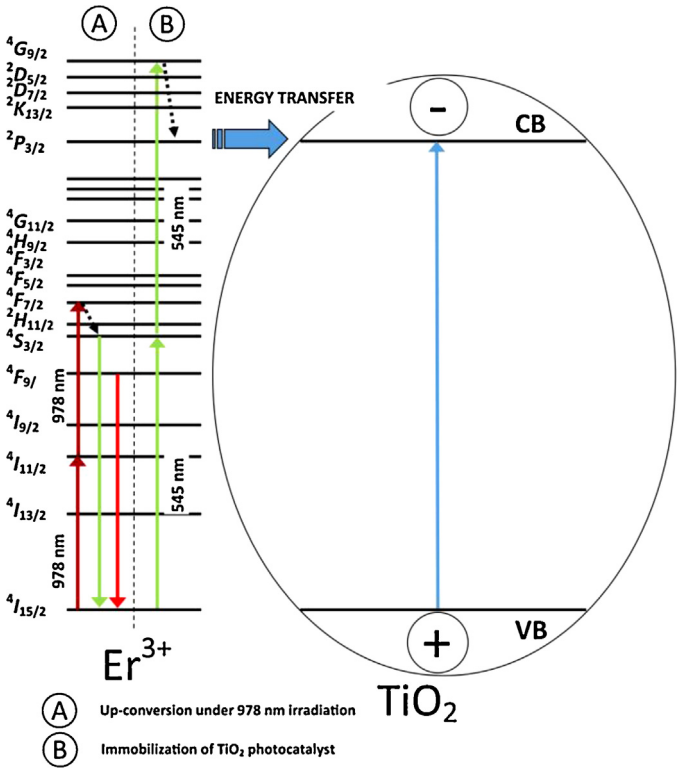

Fig. 6. Potential schematic upconversion mechanism of Er^{3+}-doped TiO_2 under 978 nm pumping.

frequently used excitation into the $^4I_{11/2}$ excited state (978 nm) resulting in the emission in vis range, also upconversion from IR to NIR can be obtained as a result of excitation of Er^{3+} ions into the $^4I_{11/2}$ excited state (1.49 μm). This phenomenon is especially interesting and investigated for solar cells applications because of the emission around 980 nm [63]. What is more, visible emission under 1.49 μm laser irradiation is also possible as a result of three photon involving process and transitions from $^2H_{11/2}/^4S_{3/2}$ and $^4F_{9/2}$ excited states into $^4I_{15/2}$ ground state [64].

One of the most important photocatalysis spectroscopic properties of Er^{3+} ions is the possibility of conversion of visible light into UV wavelengths [65–67]. This process requires the above-mentioned ESA mechanism and additionally, energy transfer between excited Er^{3+} ions (ETU, energy transfer upconversion). After excitation by light with λ = 518 nm, emission bands with maxima at 275, 318, 405, 417 and 474 nm can be observed, related to $^2H_{9/2} \rightarrow {}^4I_{15/2}$, $^2P_{3/2} \rightarrow {}^4I_{15/2}$, $^2P_{3/2} \rightarrow {}^4I_{13/2}$, $^2G_{9/2} \rightarrow {}^4I_{15/2}$ and $^2P_{3/2} \rightarrow {}^4I_{11/2}$ transitions respectively [65]. Also excitation with 647.2 nm can generate UV emission in some Er^{3+}-doped materials involving ESA and ETU mechanisms [66].

Because of the small spectral range of Er^{3+} absorption band and partially forbidden character of $^4I_{15/2}$–$^4I_{11/2}$ transition, upconversion of Er^{3+} ions obtained by GSA and ESA is ineffective. The presence of Yb^{3+} ions in the structure increases upconversion efficiency through to the energy transfer between Yb^{3+} ions, which act as sensitizers and Er^{3+}emitters. The absorption band of Yb^{3+} ions connected with $^2F_{7/2}$–$^2F_{5/2}$ transition is intense and broad, due to the strong phonon-coupling and to the relatively large Stark-splitting of the ground $^2F_{7/2}$ multiplet [68]. However, in our samples, the presence of Yb^{3+} ions had no visible effect of the registered emission. What is more, the most intense upconversion was obtained in the case of 0.25% Er^{3+}-doped sample. Generally observed greenish upconversion was low and without any dependence of the dopant composition and concentrations.

Luminescence properties of prepared RE^{3+}-doped, TiO_2 materials were checked using several excitation wavelengths covering absorption bands at IR, NIR and vis range. Only the excitation by radiation with λ = 978 nm gave characteristic for Er^{3+} ions, luminescence spectra. The emission after excitation by 545 and 660 nm was not observed which was most probably the effect of quenching properties of TiO_2. The same property was responsible for the increased photocatalytic activity of Er^{3+}-doped TiO_2. The scheme of energy transfer between Er^{3+} ions and TiO_2 is presented in Fig. 6.

The observed two emission bands after 978 nm excitation from Er^{3+} ions can be assigned to $^2H_{11/2}$, $^4S_{3/2}$–$^4I_{15/2}$ at around 545 nm and $^4F_{9/2}$–$^4I_{15/2}$ at 660 nm transitions. The energy transfer between Yb^{3+} and Er^{3+} was not observed, which suggests that these two lanthanides were in two separate phases. Also XPS results indicated that the dopants are present in such materials as oxides, which confirms our assumption. However, the ratio between emission bands at 545 and 660 nm indicated that Er^{3+} ions occupy also sites with environment different than these in rare earth oxides. For RE_2O_3 doped with Er^{3+} ions, red emission with maximum at 660 nm should be observed [69]. The ratio between green and red bands is dependent on the local environment of Er^{3+} ion and can be used for tracking structural changes of the host material. This fact and the observed expansion of TiO_2 crystal cell volume after Er^{3+} or Yb^{3+} doping confirms incorporation of dopant ions into TiO_2 crystal structure, despite unfavorable conditions of the anatase structure.

The efficiency of the upconversion luminescence depends on many factors, such as distribution of the dopant ions, their energy levels and phonon energy of the matrix. Increasing the dopant concentration can result in increased upconversion efficiency. However, too high doping level causes concentration quenching and cross relaxation, which decrease the upconversion intensity [70]. Lanthanide dopants presented mostly in synthesized materials as Er_2O_3 and Yb_2O_3 oxides are effectively quenched because of their high concentration in these phases, which is also responsible for the observed low upconversion intensity. What is more, the method of synthesis also seems to be important for upconversion. In our previous studies, concerning TiO_2 materials doped with RE^{3+} ions, synthesized by sol–gel method, upconversion was not observed [71]. Low emission intensity of Er^{3+} ions can also be an effect of interactions with TiO_2 host. Er^{3+} ions could transfer their energy to the conduction band of TiO_2 [31].

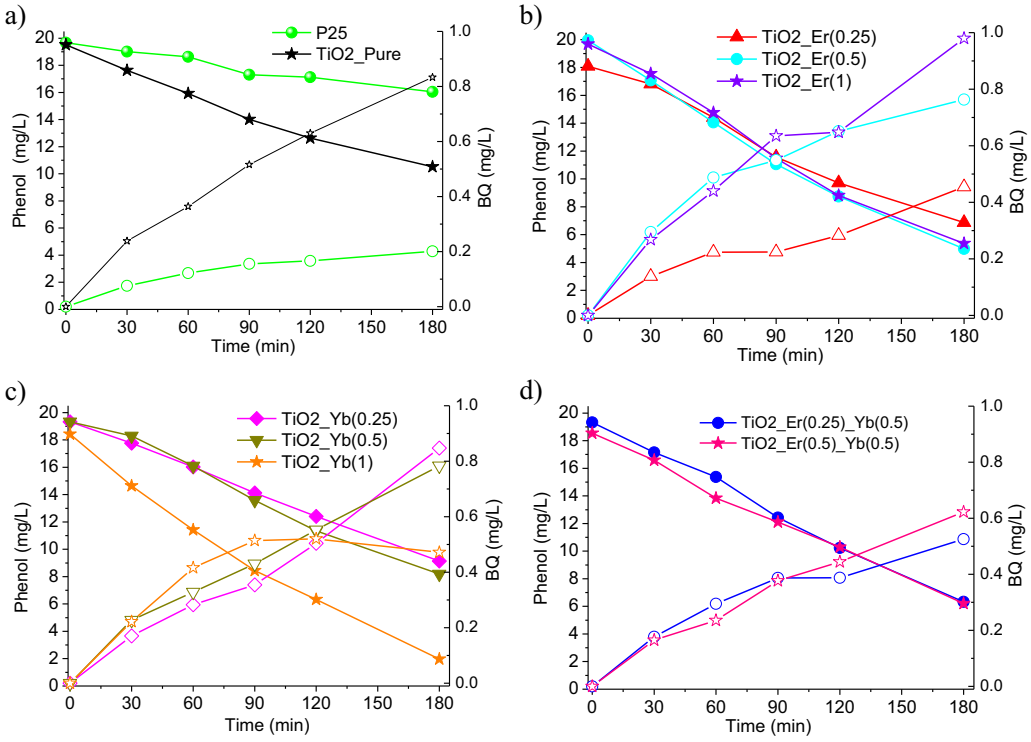

Fig. 7. Efficiency of phenol degradation and benzoquinone formation under visible light in the presence of (a) TiO_2; (b) Er-TiO_2; (c) Yb-TiO_2; (d) Er/Yb-TiO_2.

3.6. Photocatalytic activity

Photocatalytic activity of the obtained TiO_2 powders was estimated by measuring the decomposition rate of phenol in aqueous solution in the presence of visible light irradiation ($\lambda > 450$ nm). Pure TiO_2 synthesized by the sol–gel method without any dopant and P25 were used as a reference system. Kinetics of phenol photodegradation in aqueous solution under visible light irradiation in the presence of RE-doped TiO_2 nanoparticles is shown in Fig. 7 and the observed rate constants are listed in Table 4. It was found that all lanthanides-doped TiO_2 revealed higher photocatalytic activity than the undoped ones and P25. Phenol degradation rate increased from 31.89 to 58.35 μmol dm^{-3} h^{-1} for pure and Yb^{3+}-doped TiO_2, respectively. The photodegradation efficiency under visible light increased with the increase in the erbium loading up to 0.5 mol% and then decreased. After 180 min of irradiation 75% of phenol degraded for the sample TiO_2_Er(0.5). When ytterbium was used as a dopant, the photodegradation efficiency under visible light increased with the increase in metal ion concentration. The efficiency of phenol decomposition measured in the presence of the sample TiO_2_Yb(1.0) after 180 min of irradiation was 89%. It indicates that the presence of ytterbium was more beneficial for visible light activation of TiO_2 doped photocatalysts than erbium. Obtained results showed that doping with two species, Er^{3+}/Yb^{3+}, is low beneficial than doping only with one type of ions. However, the effect of Er^{3+} and Yb^{3+} amount and ratio should be systematically investigated. The 180 min irradiation by visible light resulted in 67% of phenol degradation for both TiO_2_Er(0.25)_Yb(0.5) and TiO_2_Er(0.5)_Yb(0.5) samples, and no phenol degradation for TiO_2_Er(2)_Yb(10). The sample showing the highest photoactivity under visible light irradiation was obtained by introducing of 1 mol% of Yb^{3+} during preparation step, TiO_2 was in the form of anatase, its surface area equaled to 125 m^2/g, average crystals size was 13 nm. This sample contained 0.57 wt.% of Yb^{3+} in the form of Yb_2O_3.

HPLC results showed that the main intermediate product detected after 30 min of irradiation under visible light was benzoquinone (BQ). Generally, it was observed that the concentration of BQ in the aqueous phase increased through 3 h of irradiation (Table 4, Fig. 7). Only in the case of the most active sample (e.g. TiO_2_Yb(1)), BQ concentration increased up to 90 min of irradiation and then slightly decrease due to degradation to products with smaller molecular weight. Other identified intermediate products included: hydroquinone and short-chain compounds for RE-TiO_2 and hydroquinone, catechol and short-chain compounds for P25. Their concentrations increased in the first step and decreased during the further irradiation. This means that different by-products were produced and degraded and at the same time. Similar generated intermediate products from phenol degradation were observed in literature before [44,72]. The mechanism of phenol photocatalytic destruction by studying intermediates of phenol qualitatively and in some cases quantitatively was investigated by Sobczynski et al. [73]. p-Benzoquinone can be formed in three different ways: (1) by $OH^{\bullet}$ attack on hydroquinone molecule, (2) in the reaction of the molecule with holes photogenerated in titanium dioxide; and (3) by direct oxidation of hydroquinone by oxygen dissolved in water. Further oxidation of p-benzoquinone can lead directly to oxygen-contained aliphatic compounds with no further hydroxylation of the compound [45,73].

4. Proposed mechanism

Fig. 8 illustrates the excitation of Er^{3+} under visible light, as reported by Wang et al. [74], where the absorption of 524 nm photons promotes Er^{3+} from the ground state to $^2H_{11/2}$ excited state. The upconversion process can be achieved through the chains of the ground state absorption (GSA) and excited state absorption (ESA). However, we failed to detect the UV emission when Er^{3+}-TiO_2 were irradiated with the 524 nm laser beam. Nevertheless, in order to identify the possible mechanisms of photoactivity under

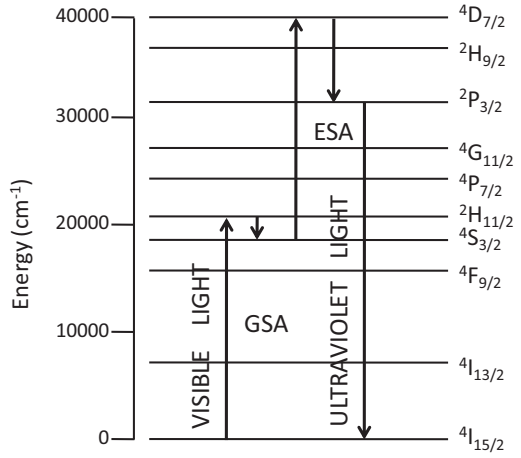

Fig. 8. Simplified energy-levels diagram of Er^{3+} and excitation path for the upconversion emission at ultraviolet light. GSA, ground state absorption; ESA, excited state absorption.

visible light irradiation, photocatalytic activity for the selected sample was investigated as a function of irradiation wavelength. Based on these studies it can be calculated which fraction of irradiation absorbed by a photocatalyst did, indeed, take part in the photocatalytic reaction. The results for the sample TiO_2_Er(0.5)_Yb(0.5) are presented in Fig. 9. The sample modified with 0.5% of Er^{3+} and 0.5% of Yb^{3+} was selected for the action spectra analysis because it contained both ions on TiO_2 surface and revealed highest photoactivity among Er/Yb-doped samples. The sample showing highest photocatalytic activity (e.g. TiO_2_Yb(1)) was not chosen since it did not show the absorption band in visible light region. RE^{3+}-TiO_2 sample gave action spectra that did not resemble the respective absorption spectra measured in a diffuse reflection mode. It is clearly seen that irradiation ranging from 420 to 475 nm is responsible for photocatalytic activity under visible light (cross-hatching area of Fig. 9). There is no higher activity observed for wavelength 524 nm, characteristic for the presence of rare earth metals. Thus, the upconversion effect was not observed for the TiO_2_Er(0.5)_Yb(0.5) sample. Castañeda-Contreras et al. [31] reported photodegradation of methylene blue under 532 nm laser beam light in the presence

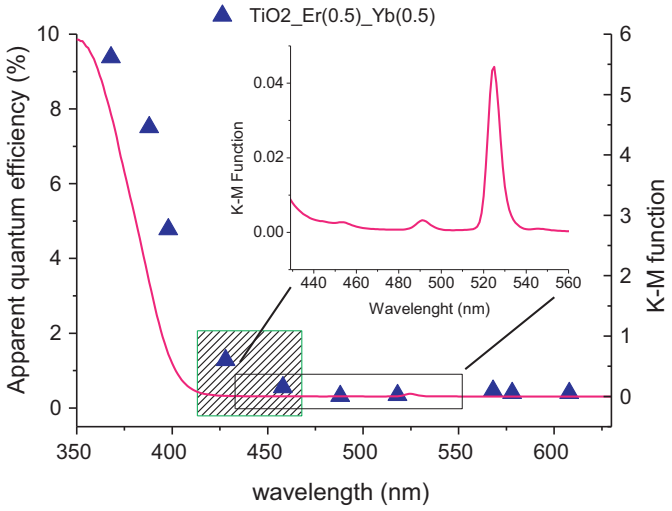

Fig. 9. Action spectrum of acetic acid oxidation on erbium/ytterbium modified TiO_2 and absorption spectrum of sample. Cross-hatching area is responsible for photocatalytic activity under visible light irradiation.

of Er^{3+}-TiO_2 nanoparticles. They attributed the sensitization of the nanoparticles to visible light to a red shift in the band-gap of the TiO_2 due to the addition of erbium ions.

Observed higher photoactivity could be affected both by the presence of oxygen vacancies, higher absorption in visible region, as well as better adsorption capacities of doped TiO_2 than a pure one. It is well know that electron–hole separation is one of the key factors limiting the efficiency of the photocatalytic process. Obtained results suggested that Ti^{4+} ions in the lattices of titania could be substituted by Er^{3+} and Yb^{3+}, creating abundant oxygen vacancies and surface defects for electron trapping and pollutant adsorption, accelerating the separation of photogenerated electron–hole pairs and organic pollutant photodegradation. The formation of an excitation energy level below the conduction band of TiO_2 from the binding of electrons and oxygen vacancies decreases the excitation energy of RE doped TiO_2, resulting in highly active photocatalysts [75]. The efficiency of charge carrier trapping, migration, and transfer and better understanding the fate of electron–hole pair in semiconductor particles could be investigated using PL emission spectra [76]. Thus, based on the PL emission spectra analysis shown in Fig. 4, it could be assumed that doping with Er^{3+} and Yb^{3+} generally decrease PL intensity, which clearly indicates that the presence of these species induces a suppression of the recombination process of photogenerated electrons and holes. Only the TiO_2_Er(2)_Yb(10) sample, which is not active in phenol degradation reaction, shows higher PL intensity than pure TiO_2.

On the other hand, recent literature reported also the ability of lanthanides to form complexes with various Lewis bases e.g. acids, amines, aldehydes, alcohols, thiols, etc. in the interaction of these functional groups with the f-orbitals of the lanthanides [77]. Thus, incorporation of lanthanide ions in a TiO_2 matrix could provide capabilities to concentrate the organic pollutants at the semiconductor surface. Our results clearly indicated, that efficiency of phenol adsorption at the surface of doped TiO_2 is more than 6 times of that pure one. The most active sample revealed more than 3 times higher adsorption efficiency of phenol than pure TiO_2.

Summarizing, the primary mechanism for the visible light sensitization was probably due to the availability of higher adsorption sites, increase of the BET surface area, decrease of the crystallite size and prevention of electron–hole recombination. This affirmation is in agreement with that of Parida and Sahu [78]. The visible-light sensitization promoted an electron from TiO_2 valence band to the conduction band. The generated charge carriers produced oxidative species, such as hydroxyl radicals that degraded phenol and acetone in aqueous solution.

5. Conclusions

Visible light-activated anatase system was obtained by doping with Er^{3+}, Yb^{3+} and Er^{3+}/Yb^{3}. XPS analysis revealed that erbium and ytterbium were present in the form of oxides. For TiO_2 materials doped with Er^{3+} or Yb^{3+}/Er^{3+} after excitation by 978 nm laser beam, low intensive upconversion emission was observed. Yb^{3+}-TiO_2 containing 1 mol% ytterbium, exhibits the highest photocatalytic activity under visible light ($\lambda > 450$ nm) irradiation. Action spectra analysis showed that RE^{3+}-doped TiO_2 could be excited under visible light in the range from 420 to 475 nm. The primary mechanism for the visible light sensitization was probably due to the availability of higher adsorption sites, increase of the BET surface area, decrease of the crystallite size and prevention of electron–hole recombination. Luminescence properties of Er/Yb-TiO_2, as well as XRD analysis, indicates incorporation of dopant ions into TiO_2 crystal structure creating oxygen vacancies and surface defects.

Acknowledgements

This research was financially supported by Polish National Science Center (grant no. 2011/01/N/ST5/05537). One of us (T. Grzyb) holds a scholarship from the Foundation for Polish Science for Young Scientists (FNP).

References

[1] M. Nischk, P. Mazierski, M. Gazda, A. Zaleska, Appl. Catal. B 144 (2013) 674–685.
[2] W. Wang, M. Ding, C. Lu, Y. Ni, Z. Xu, Appl. Catal. B 144 (2013) 379–385.
[3] A. Zaleska, Recent Pat. Eng. 2 (2008) 157–164.
[4] D. Dolat, S. Mozia, B. Ohtani, A.W. Morawski, Chem. Eng. J. 225 (2013) 358–364.
[5] K. Sridharan, E. Jang, T. Park, Appl. Catal. B 142–143 (2013) 718–728.
[6] J. Santiago-Morales, A. Agüera, M. Gómez, A. Fernández-Alba, J. Giménez, S. Esplugas, R. Rosal, Appl. Catal. B 129 (2013) 13–29.
[7] Y. Cong, B. Tian, J. Zhang, Appl. Catal. B 101 (2011) 376–381.
[8] E. Grabowska, A. Zaleska, S. Sorgues, M. Kunst, A. Etcheberry, H. Remita, J. Phys. Chem. C 117 (2013) 1955–1962.
[9] M. Bellardita, A. Di Paola, L. Palmisano, F. Parrino, G. Buscarino, R. Amadelli, Appl. Catal. B 104 (2011) 291–299.
[10] S. Ramya, S.D. Ruth Nithila, R.P. George, D.N.G. Krishna, C. Thinaharan, U. Kamachi Mudali, Ceram. Int. 39 (2013) 1695–1705.
[11] H. Shi, T. Zhang, T. An, B. Li, X. Wang, J. Colloid Interface Sci. 380 (2012) 121–127.
[12] D. Lee, J. Kim, J. Park, Y. Kim, I. Lee, M. Lee, B. Kim, Curr. Appl. Phys. (2013) 1–5.
[13] J. Méndez-Ramos, P. Acosta-Mora, J.C. Ruiz-Morales, N.M. Khaidukov, J. Alloys Compd. 575 (2013) 263–267.
[14] Y. Badr, I.K. Battisha, A. Salah, M.A. Salem, Indian J. Pure Appl. Phys. 46 (2008) 706–711.
[15] A. Bahtat, M. Bouazaoui, M. Bahtat, C. Garapon, B. Jacquier, J. Mugnier, J. Non-Cryst. Solids 202 (1996) 16–22.
[16] I.K. Battisha, J. Non-Cryst. Solids 353 (2007) 1748–1754.
[17] I. Cacciotti, A. Bianco, G. Pezzotti, G. Gusmano, Chem. Eng. J. 166 (2011) 751–764.
[18] B.S. Cao, Y.Y. He, Z.Q. Feng, M. Song, B. Dong, Opt. Commun. 28 (2011) 3311–3314.
[19] J. Castaneda, J. Rare Earth 29 (2011) 420–425.
[20] J. Castañeda-Contreras, M.a. Meneses-Nava, O. Barbosa-García, J.L. Maldonado-Rivera, J.F. Mosiño, Opt. Mater. 27 (2004) 301–305.
[21] K.L. Frindell, M.H. Bartl, M.R. Robinson, G.C. Bazan, A. Popitsch, G.D. Stucky, J. Solid State Chem. 172 (2003) 81–88.
[22] T. Ji, Y. Liu, H. Zhao, H. Du, J. Sun, G. Ge, J. Solid State Chem. 183 (2010) 584–589.
[23] X. Mao, B. Yan, J. Wang, J. Shen, Vacuum 102 (2014) 38–42.
[24] L. Liang, Y. Yulin, Z. Mi, F. Ruiqing, Q. LeLe, W. Xin, Z. Lingyun, Z. Xuesong, H. Jianglong, J. Solid State Chem. 198 (2013) 459–465.
[25] X. Pan, J. Yu, Y. Liu, S. Yoda, M. Zhang, F. Ai, F. Jin, H. Yu, W. Jin, J. Lumin. 132 (2012) 1025–1029.
[26] S. Pang, X. Li, Z. Shi, G. Yang, Z. Cui, Mater. Lett. 64 (2010) 846–848.
[27] A. Patra, C. Friend, R. Kapoor, P.N. Prasad, Chem. Mater. 15 (2003) 3650–3655.
[28] Q. Shang, H. Yu, X. Kong, H. Wang, X. Wang, Y. Sun, Y. Zhang, Q. Zeng, J. Lumin. 128 (2008) 1211–1216.
[29] H. Wang, Y. Wang, Y. Yang, X. Li, C. Wang, Mater. Res. Bull. 44 (2009) 408–414.
[30] J. Zhang, H. Tao, Y. Cheng, X. Zhao, J. Rare Earth 25 (2007) 108–112.
[31] J. Castañeda-Contreras, V.F. Marañón-Ruiz, R. Chiu-Zárate, H. Pérez-Ladrón de Guevara, R. Rodriguez, C. Michel-Uribe, Mater. Res. Bull. 47 (2012) 290–295.
[32] G. Feng, S. Liu, Z. Xiu, Y. Zhang, J. Yu, Y. Chen, P. Wang, X. Yu, J. Phys. Chem. C 112 (2008) 13692–13699.
[33] C.-H. Liang, M.-F. Hou, S.-G. Zhou, F.-B. Li, C.-S. Liu, T.-X. Liu, Y.-X. Gao, X.-G. Wang, J.-L. Lü, J. Hazard. Mater. 138 (2006) 471–478.
[34] J. Wang, R. Li, Z.H. Zhang, W. Sun, R. Xu, Y. Xie, Z. Xing, X. Zhang, Appl. Catal. A 334 (2008) 227–233.
[35] Y. Yang, C. Zhang, Y. Xu, X. Wang, X. Li, C. Weng, Mater. Lett. 64 (2010) 147–150.
[36] A.W. Xu, Y. Gao, H.Q. Liu, J. Catal. 207 (2002) 151–157.
[37] Y. Zheng, W. Wang, J. Solid State Chem. 210 (2014) 206–212.
[38] D. Hou, R. Goei, X. Wang, P. Wang, T. Lim, Appl. Catal. B 126 (2012) 121–133.
[39] J. Reszczynska, A. Iwulska, G. Śliwinski, A. Zaleska, Physicochem. Probl. Miner. Process. 48 (2012) 201–208.
[40] S. Obregon, A. Kubacka, M. Fernández-García, G. Colón, J. Catal. 299 (2013) 298–306.
[41] B. Ohtani, Chem. Lett. 37 (2008) 216–230.
[42] R.J. Hill, C.J. Howard, Australian Atomic Energy Commission Research Report M112, 1986.
[43] M. Horn, C.F. Schwerdtfeger, E.P. Meagher, Kristallgeometrie, Kristallphysik, Kristallchemie 136 (1972) 273–281.
[44] A. Zielinska-Jureka, E. Kowalska, J.W. Sobczak, W. Lisowski, B. Ohtani, A. Zaleska, Appl. Catal. B 101 (2011) 504–514.
[45] E. Grabowska, J. Reszczynska, A. Zaleska, Water Res. 46 (2012) 5453–5471.
[46] P. Yan, H. Jiang, S. Zang, J. Li, Q. Wang, Q. Wang, Mater. Chem. Phys. 139 (2013) 1014–1022.
[47] R. Guo, Y.C. Wu, P.Z. Fu, F.L. Jing, Chem. Phys. Lett. 416 (2005) 133–136.
[48] V. Swamy, D. Menzies, B.C. Muddle, A. Kuznetsov, L.S. Dubrovinsky, Q. Dai, V. Dmitriev, Appl. Phys. Lett. 88 (2006) 243103.
[49] H. Zhang, B. Chen, J.F. Banfield, PCCP 11 (2009) 2553–2558.
[50] W. Luo, R. Li, G. Liu, M.R. Antonio, X. Chen, J. Phys. Chem. C 112 (2008) 10370–10377.
[51] Ţ. Antic, R.M. Krsmanovic, M.G. Nikolic, M. Marinovic-Cincovic, M. Mitric, S. Polizzi, M.D. Dramicanin, Mater. Chem. Phys. 135 (2012) 1064–1069.
[52] Z. El-bahy, A. Ismail, R. Mohamed, J. Hazard. Mater. 166 (2009) 138–143.
[53] P. Gorska, A. Zaleska, E. Kowalska, T. Klimczuk, J.W. Sobczak, E. Skwarek, W. Janusz, J. Hupka, Appl. Catal. B 84 (2008) 440–447.
[54] H. Jensen, A. Soloviev, Z. Li, E.G. Sogaard, Appl. Surf. Sci. 246 (2005) 239–249.
[55] P.J. Cumpson, M.P. Seah, Surf. Interface Anal. 25 (1997) 430–446.
[56] K.T. Ranjit, H. Cohen, I. Willner, S. Bossmann, M. Braun, J. Mater. Sci. 34 (1999) 5273–5280.
[57] Y.A. Teterin, A.Y. Teterin, Russ. Chem. Rev. 71 (2002) 347–381.
[58] A. Rjeb, S. Letarte, L. Tajounte, M. Chafik El Idrissi, A. Adnot, D. Roy, Y. Claire, J. Kaloustian, J. Electron. Spectrosc. Relat. Phenom. 107 (2000) 221–230.
[59] J. Yu, X. Zhao, Q. Zhao, Thin Solid Films 379 (2000) 7–14.
[60] F. Auzel, Chem. Rev. 104 (2004) 139–174.
[61] T. Wen, W. Luo, Y. Wang, M. Zhang, Y. Guo, J. Yuan, J. Ju, Y. Wang, F. Liao, B. Yang, J. Mater. Chem. C 1 (2013) 1995–2001.
[62] M. Nyk, R. Kumar, T.Y. Ohulchanskyy, E.J. Bergey, P.N. Prasad, Nano Lett. 8 (2008) 3834–3838.
[63] R. Martín-Rodríguez, S. Fischer, A. Ivaturi, B. Froehlich, K.W. Kramer, J.C. Goldschmidt, B.S. Richards, A. Meijerink, Chem. Mater. 25 (2013) 1912–1921.
[64] G. Chen, T.Y. Ohulchanskyy, A. Kachynski, H. Agren, P.N. Prasad, ACS Nano 5 (2011) 4981–4986.
[65] H.G. Yang, Z.W. Dai, Z.W. Sun, Chin. Phys. 15 (2006) 1273.
[66] H.G. Yang, Z.W. Dai, N.N. Zu, Chin. Phys. 16 (2007) 1650–1655.
[67] J. Zheng, X.F. Wang, W.Y. He, Y.Y. Bu, X.H. Yan, Appl. Phys. B 1 (2013) 1–7.
[68] I. Sokolska, W. Ryba-Romanowski, S. Gołab, T. Lukasiewicz, Appl. Phys. B 65 (1997) 495–498.
[69] Z. Liu, Z. Li, J. Liu, S. Gu, Q. Yuan, J. Ren, X. Qu, Biomaterials 33 (2012) 6748–6757.
[70] T. Grzyb, A. Gruszeczka, R.J. Wiglusz, S. Lis, J. Mater. Chem. C 1 (2013) 5410–5418.
[71] J. Reszczynska, T. Grzyb, J.W. Sobczak, W. Lisowski, M. Gazda, B. Ohtani, A. Zaleska, Appl. Surf. Sci. 307 (2014) 333–345.
[72] B. Tryba, A.W. Morawski, M. Inagaki, M. Toyoda, J. Photochem. Photobiol. A: Chem. 179 (2006) 224–228.
[73] A. Sobczynski, L. Duczmal, W. Zmudzinski, J. Mol. Catal. A: Chem. 213 (2004) 225–230.
[74] J. Wang, Y. Xie, Z.H. Zhang, J. Li, C. Li, L. Zhang, Z. Xing, R. Xu, X. Zhang, Environ. Chem. Lett. 8 (2008) 87–93.
[75] Y. Chai, L. Lin, K. Zhang, B. Zhao, D. He, Ceram. Int. 40 (2014) 2691–2696.
[76] D. Li, H. Haneda, S. Hishita, N. Ohashi, Chem. Mater. 17 (2005) 2596–2602.
[77] K.T. Ranjit, I. Willner, S.H. Bossmann, A.M. Braun, Environ. Sci. Technol. 35 (2001) 1544–1549.
[78] K.M. Parida, N. Sahu, J. Mol. Catal. A: Chem. 287 (2008) 151–158.